



## Synthesis, Spectral Characterization, Docking Analysis, DNA Binding/Cleavage, Antimicrobial and Cytotoxic Activity of New Dimeric Antipyrene-Schiff Base Metal Complexes

ABDEL-NASSER M.A. ALAGHAZ<sup>1\*</sup>, AMANI S. ALTURIQI<sup>2</sup>, REDA A. AMMAR<sup>3</sup> and MOHAMED E. ZAYED<sup>4</sup>

<sup>1</sup>Department of Chemistry, College of Science, Jazan University, Jazan, Saudi Arabia

<sup>2</sup>Department of Chemistry, College of Science, Princess Nourah Bint Abdul Rahman University, Riyadh, Saudi Arabia

<sup>3</sup>Department of Chemistry, College of Science, Al-Imam Mohammad Ibn Saud Islamic University, Riyadh, Saudi Arabia

<sup>4</sup>Department of Botany and Microbiology, Faculty of Science, King Saud University, Riyadh 11541, Saudi Arabia

\*Corresponding author: E-mail: aalajhaz@hotmail.com

Received: 28 August 2018;

Accepted: 24 September 2018;

Published online: 30 November 2018;

AJC-19183

In the present study, a new series of novel Schiff base ligand derived from (furan-2-carbaldehyde and 4-aminoantipyrene) and dimeric metal(II) complexes with the composition of  $[MLCl_2]_2$ , where M=Cu(II), Co(II), Ni(II) and Zn(II) have been synthesized and characterized by elemental analysis, magnetic susceptibility, molar conductivity measurements, FT-IR, UV-visible, <sup>1</sup>H NMR, <sup>13</sup>C NMR, EPR, MS (ESI), XRD, SEM and EDX studies. The spectral data recommend that the dimeric metal complexes embrace octahedral geometry around the central metal ions. The DMF solutions of the dimeric metal complexes demonstrate the lower molar conductance values which might be due to the non-electrolytic nature of the complexes ( $5.67-13.24 \Omega^{-1} \text{ mol}^{-1} \text{ cm}^2$ ). The biological studies involved are DNA interaction (binding and damage) antimicrobial, anti-proliferative and molecular docking. DNA interaction of these complexes carried out with using calf thymus DNA (CT-DNA) by electronic absorption titration, viscometric measurement which revealed that the synthesized dimeric complexes interact with DNA through intercalative binding mode. A gel electro-phoresis assay testifies the ability of complexes to cleave supercoiled pUC19 DNA in the presence of hydrogen peroxide as an activator. The synthesized compounds were initiated from their biological perspective. The antimicrobial assay indicates that dimeric complexes are good antimicrobial agents. Besides, *in vitro* antiproliferative activity of dimeric complexes were investigated on MCF-7, Hep G2, HBL-100 cell lines using an MTT assay. In addition, the molecular docking study was accomplished to considerate the nature of binding of the synthesized compounds with protein and DNA.

**Keywords:** Dimeric Schiff base complexes, Magnetic susceptibility, DNA binding, Antiproliferative activity, Molecular docking.

### INTRODUCTION

Schiff bases are considered an important class of ligands because they exhibit synthetic flexibility in addition to being selective regarding the central metal atom and sensitive to it. In coordination chemistry, Schiff bases are known as privileged ligands because they are prepared using simple condensation reactions between aldehydes and primary amines [1,2]. The azomethine (HC=N) group of a Schiff base ligand is primarily responsible for coordination of metal ions through the lone pair of electrons presents on N atom. Currently, Schiff bases constitute an active area of research primarily because they have numerous and diverse applications in optical material produc-

tion, drug design, catalysis and in the production of biological probes and chemical sensors [3-6]. Stable complexes are formed by the combination of Schiff bases and various transitions and inner transition metals. Most of the metal complexes have recently been tested by several bioinorganic chemists for determining and quantifying their anticancer properties [7-10]. DNA damage is the major cause of cancer; strategies for controlling DNA damage constitute the prime focus area for cancer related research [11]. Many currently used chemotherapeutic agents are reported to curb tumor growth by interfering with DNA replication and transcription. In living cells, the primary function of DNA is the storage and transport of genetic codes in a cell. Furthermore DNA is a crucial target for drugs that are involved

in the intercellular control of cancer [12,13]. Different sequences in the DNA are involved in various regulatory processes, such as gene transcription, gene expression, carcinogenesis and mutagenesis [14]. Interactions between metal complexes and DNA may cause modifications in the DNA sequences, thereby causing DNA damage. Zuber *et al.* [15] reported that the interaction between small molecules and DNA can cause DNA damage. In addition, it prevents cell division in cancer cells, which results in cancer cell death [15].

4-Aminoantipyridine and its derivatives have myriad of applications in catalysis, pharmacology and medicine [16-18]. Understanding the factors involved in drug development and drug innovation is necessary for progress in health care as well as future research and development in drug identification. New types of chemotherapeutic agents containing Schiff bases have generated tremendous interest among biochemists and some aminopyridines are commonly administered intravenously for the diagnosis of liver diseases in clinical practice [19-22]. To probe their chemotherapeutic functions, applications and properties, several 4-aminoantipyridine based agents are routinely administered intravenously for the diagnosis of liver diseases at diagnostic centers [23]. Chromosensors are widely used for environmental monitoring and in industrial and biological processes; consequently, research efforts are now being directed toward designing and developing sensitive yet simple 4-aminoantipyridine based chromosensors. 4-Aminoantipyridine was used as a key intermediate for the synthesis of heterocyclic compounds with biologically active moieties [24]. 4-Aminoantipyridine administration led to a constant reduction in the contracture of myometrium, whereas the cervix did not exhibit any major effect [25]. Previous studies [26,27] have explored binding reactions among 4-aminoantipyridine, human serum albumin and DNA. 4-Aminoantipyridine derivatives are well-known sensors in clinical practice. However, studies examining their activity against cervical cancer are not currently available. In this study, coordination behaviour of 4-aminoantipyridine ligand was altered using condensation reactions involving aldehydes, ketones, thiosemicarbazides and carbazides to obtain a flexible ligand system. In this study, we reported the synthesis, characterization, antimicrobial, molecular docking and cytotoxic studies of novel transition metal complexes containing Schiff bases derived from 4-aminoantipyridine and furan-2-carbaldehyde.

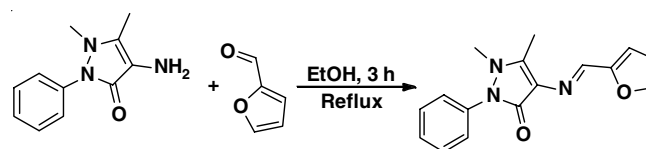
## EXPERIMENTAL

In this research work, the chemicals were used as AnalaR grade without further purification. However, the solvent is used as a purified solvent by distillation method. The reagents are furan-2-carbaldehyde and 4-aminoantipyridine was procured from Sigma Aldrich India. All other metal chloride salts were collected from Merck products.

Metal contents were determined complexometrically by standard EDTA titration and chloride content was tested gravimetrically using AgNO<sub>3</sub>. Vibration spectral data has been derived by using FT-IR Shimadzu model IR-Affinity-1 spectrophotometer using KBr discs. <sup>1</sup>H NMR and <sup>13</sup>C NMR spectral data of ligand and their dimeric Zinc(II) complex were recorded by using Bruker 400MHz Advance III HD Nanobay NMR spectrometer with DMSO-*d*<sub>6</sub> as a deuterated solvent. Mass spectra were

obtained on a JEOL JMS-D300 mass spectrometer (scan range, mass-to-charge (*m/z*) ratio 0-850) at Venture Business Laboratory, University of Toyama, Japan. The molar conductivity of complexes in DMF (10<sup>-3</sup> M) solution was measured at room temperature using deep vision 601 model digital conductivity meter. The X-band of EPR spectrum was recorded at LNT (77 K) and room temperature (300 K). Absorption spectra were recorded using UV-visible spectrophotometer (Shimadzu model UV-1601) at room temperature. The X-ray diffraction study of dimeric Cu(II), Co(II), Ni(II) and Zn(II) complexes were recorded on a Phillips PW 1130/00 diffractometer with scan axis-Gonio, start position (2θ-10.004) end position (2θ-89.976) anode material CuKα ALPHA λ = 1.54060 Å and the generator settings 30mA, 40 KV. Surface morphology was studied by a field emission Scanning Electron Microscopy (SEM) (Model SUPRA 40) with a voltage of 30 KV. Energy Dispersive X-ray (EDX) analysis was done by EDX (TESCAN) X-max version 4.1.17.D /Mi 152. The TG, DTG and DTA of Co(II) complex is recorded on NETZSCH STA 409 C/CD in nitrogen atmosphere at a heating rate of 10 °C/min.

**Synthesis of Schiff base (L):** Schiff base ligand (L) was synthesized by modifying the procedure of Zhou *et al.* [28] by dissolving 5 mmol of 4-aminoantipyridine in 20 mL of ethanol and 5 mmol of furan-2-carbaldehyde in 20 mL of ethanol. The mixture of two reactants was stirred for 5 h. The solvent was then reduced to one-third of its volume and the resultant yellow solid product was filtered and recrystallized from ethanol and dried in vacuum at room temperature (Scheme-I).

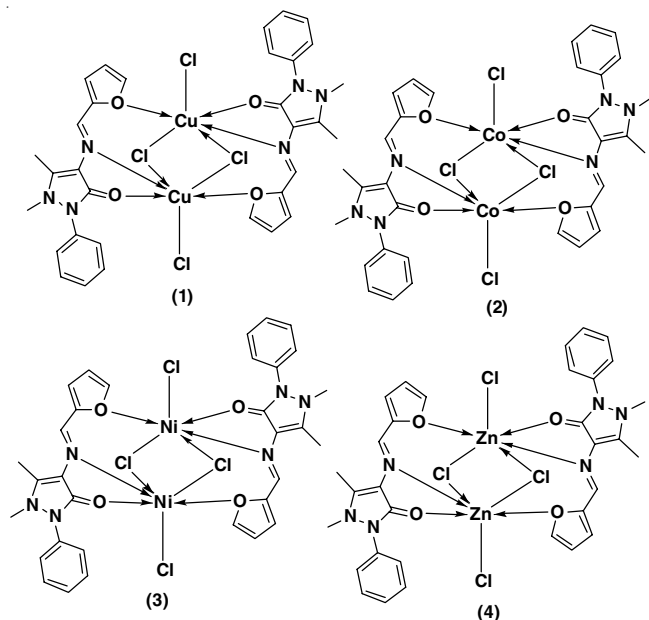


Scheme-I: Synthesis of Schiff's base ligand (L)

**Synthesis of 4-(furan-2-ylmethyleneamino)-1,5-dimethyl-2-phenyl-1,2-dihydro-3H-pyrazol-3-one (L):** Yield: 92 %. m.f. C<sub>16</sub>H<sub>15</sub>N<sub>3</sub>O<sub>2</sub>; colour: yellow; Anal. cald. (found) %: C, 68.31 (68.28), H, 5.37 (5.32), N, 14.94 (14.91). FT-IR (KBr,  $\nu_{\max}$ , cm<sup>-1</sup>): 1638 (-C=O), 1586 (-CH=N), 1027 (-C-O-C), ring vibrations 1584, 1012, 923, 734, 727, 674, 607, 542, 444. <sup>1</sup>H NMR (DMSO-*d*<sub>6</sub>) ( $\delta$ , ppm): 2.4 (s, 3H, C-CH<sub>3</sub>), 3.1 (s, 3H, N-CH<sub>3</sub>), 7.8-6.8 (m, 8, ArH & hetero-H), 8.3 (s, 1H, -CH=N). <sup>13</sup>C NMR (DMSO-*d*<sub>6</sub>) ( $\delta$ , ppm): 10.4 (s, 1C, C-CH<sub>3</sub>), 36.8 (s, 1C, N-CH<sub>3</sub>), 55.3-136.8 (m, 13, Ar-C & hetero-C), 145.7 (s, 1C, -C-O-), 152.2 (s, 1C, C=O), 161.2 (s, 1C, -CH=N); ESI-MS: 281 (molecular ion peak).

**Synthesis of dimeric metal(II) complexes:** To synthesize Schiff base metal complexes, Schiff base ligand (2 mmol) and their corresponding metal chloride salt (2 mmol) were mixed with 2:2 portion in hot ethanol (50 mL), then it was allowed to stir with reflux for 8 h. The resultant product was washed with ethanol, filtered and then recrystallized. The obtained solid product was dried over anhydrous CaCl<sub>2</sub> under vacuum condition (Scheme-II).

**Synthesis of [Cu<sub>2</sub>( $\mu$ -Cl)<sub>2</sub>[(4-(furan-2-ylmethyleneamino)-1,5-dimethyl-2-phenyl-1,2-dihydro-3H-pyrazol-3-one)<sub>2</sub>Cl<sub>2</sub>]] (1) [CuLCl<sub>2</sub>]<sub>2</sub>:** Yield: 78 %, m.w. 831.5, colour: brown.



Scheme-II: Proposed structures of dimeric Schiff base complexes

Anal. calcd. (found) % for  $C_{32}H_{30}N_6O_4Cl_4Cu_2$ : C, 46.17 (46.22); H, 3.65 (3.64); Cl, 16.95 (17.05); N, 10.08 (10.11); Cu, 15.24 (15.28).  $\Lambda_m \times 10^{-3}$  (DMF,  $\Omega^{-1} \text{ mol}^{-1} \text{ cm}^{-2}$ ): 13.24; BM: 1.87. UV-visible (EtOH):  $\lambda_{\text{max}}$ , nm ( $\epsilon$ ,  $\text{L mol}^{-1} \text{ cm}^{-1}$ ): 617 (23843). FT-IR (KBr,  $\nu_{\text{max}}$ ,  $\text{cm}^{-1}$ ): 1667 (C=O), 1592 (-CH=N), 1008 (-C-O-C), 537 (M-O), 427 (M-N), ring vibrations 1608, 1018, 858, 745, 693, 632, 579, 531, 442. ESI-MS:  $m/z$  831 ( $M^+$ ).

**Synthesis of  $[Co_2(\mu-Cl)_2((4\text{-furan-2-ylmethyleneamino-1,5-dimethyl-2-phenyl-1,2-dihydro-3H-pyrazol-3-one})_2Cl_2)]$  (2)  $[CoLCl_2]_2$ :** Yield: 89.7 %, m.w. 822.3, colour: pink. Anal. calcd. (found) % for  $C_{32}H_{30}N_6O_4Cl_4Co_2$ : C, 46.74 (46.72); H, 3.68 (3.66); Cl, 17.24 (17.21); N, 10.22 (10.24); Co, 14.33 (14.30).  $\Lambda_m \times 10^{-3}$  (DMF,  $\Omega^{-1} \text{ mol}^{-1} \text{ cm}^{-2}$ ): 10.32; BM: 5.18. UV-visible (EtOH):  $\lambda_{\text{max}}$ , nm ( $\epsilon$ ,  $\text{L mol}^{-1} \text{ cm}^{-1}$ ): 614 (24847). FT-IR (KBr,  $\nu_{\text{max}}$ ,  $\text{cm}^{-1}$ ): 1645 (C=O), 1590 (-CH=N), 1010 (-C-O-C), 522 (M-O), 427 (M-N), ring vibrations 1602, 1014, 853, 742, 696, 634, 575, 534, 448. ESI-MS:  $m/z$  822 ( $M^+$ ).

**Synthesis of  $[Ni_2(\mu-Cl)_2((4\text{-furan-2-ylmethyleneamino-1,5-dimethyl-2-phenyl-1,2-dihydro-3H-pyrazol-3-one})_2Cl_2)]$  (2)  $[NiLCl_2]_2$ :** Yield: 89.8 %, m.w. 821.8, colour: green. Anal. calcd. (found) % for  $C_{32}H_{30}N_6O_4Cl_4Ni_2$ : C, 46.77 (46.72); H, 3.68 (3.64); Cl, 17.25 (17.23); N, 10.23 (10.21); Ni, 14.28 (14.25).  $\Lambda_m \times 10^{-3}$  (DMF,  $\Omega^{-1} \text{ mol}^{-1} \text{ cm}^{-2}$ ): 8.61; BM: 2.89. UV-visible (EtOH):  $\lambda_{\text{max}}$ , nm ( $\epsilon$ ,  $\text{L mol}^{-1} \text{ cm}^{-1}$ ): 624 (21843). FT-IR (KBr,  $\nu_{\text{max}}$ ,  $\text{cm}^{-1}$ ): 1639 (C=O), 1598 (-CH=N), 1014 (-C-O-C), 537 (M-O), 423 (M-N), ring vibrations 1604, 1021, 857, 746, 658, 639, 573, 535, 449. ESI-MS:  $m/z$  821 ( $M^+$ ).

**Synthesis of  $[Zn_2(\mu-Cl)_2((4\text{-furan-2-ylmethyleneamino-1,5-dimethyl-2-phenyl-1,2-dihydro-3H-pyrazol-3-one})_2Cl_2)]$  (2)  $[ZnLCl_2]_2$ :** Yield: 88.3 %, m.w. 821.8, colour: pale yellow. Anal. calcd. (found) % for  $C_{32}H_{30}N_6O_4Cl_4Zn_2$ : C, 46.02 (46.00); H, 3.62 (3.61); Cl, 16.98 (16.93); N, 10.06 (10.02); Zn, 15.66 (15.64).  $\Lambda_m \times 10^{-3}$  (DMF,  $\Omega^{-1} \text{ mol}^{-1} \text{ cm}^{-2}$ ): 5.67;  $\mu_{\text{eff}}$ : diamagnetic. UV-visible (EtOH):  $\lambda_{\text{max}}$ , nm ( $\epsilon$ ,  $\text{L mol}^{-1} \text{ cm}^{-1}$ ): 265 (35720). FT-IR (KBr,  $\nu_{\text{max}}$ ,  $\text{cm}^{-1}$ ): 1633 (C=O), 1591 (CH=N), 1012 (-C-O-C), 523 (M-O), 444 (M-N).  $^1\text{H NMR}$  (DMSO- $d_6$ ) ( $\delta$ , ppm):

2.4 (s, 6, C-CH<sub>3</sub>), 3.1 (s, 6, N-CH<sub>3</sub>), 7.8-6.8 (m, 16, ArH & hetero-H), 9.1 (s, 2H, -CH=N).  $^{13}\text{C NMR}$  (DMSO- $d_6$ ) ( $\delta$ , ppm): 10.5 (s, 2C, C-CH<sub>3</sub>), 36.4 (s, 2C, N-CH<sub>3</sub>), 55.2-136.3 (m, 26, ArC & hetero-C), 149.8 (s, 4C, C-O-C), 154.3 (s, 2C, C=O), 168.2 (s, 2C, CH=N), ring vibrations 1598, 1023, 855, 748, 688, 635, 576, 542, 448. ESI-MS:  $m/z$  835 ( $M^+$ ).

**DNA binding experiments:** In absorption spectral studies, the intrinsic binding constant ( $K_b$ ) value of these complexes are obtained by using the medium of 5 mM tris-HCl/50 mM NaCl buffer (pH 7.2), DNA stock solution and fixed concentration solution of metal complexes in DMSO. These absorption spectra were recorded on a Shimadzu model UV-1601 spectrophotometer using cuvettes having 1 cm path length. The concentrated stock solution of metal complexes was diluting suitable with corresponding buffer solution to required concentrations for all experiments and the spectra of these complexes were recorded before and after the addition of DNA [29]. The interaction of each complex with DNA was obtained from absorption data. These absorption spectral titrations were performed by the incremental addition of nucleic acid to constant concentration of the complex. This titration process was repeated until there is no change in the absorption values, suggesting the binding saturation.

**Viscosity measurements:** Viscosity measurements of all the metal complexes were carried out by Ostwald viscometer, at a constant temperature  $30.0 \pm 0.1$  °C by using thermostat water-bath. Approximately 0.5mM sample of CT-DNA were prepared by sonication in order to minimize the complexities arising from CT-DNA flexibility [30]. Flow time was measured for all the metal complexes in thrice using the digital stopwatch and an average flow time was calculated at both pH. The data were calculated against  $\eta/\eta_0$  and the concentration of metal(II) complexes, where  $\eta$  is indicated as the viscosity of CT-DNA with metal complexes and  $\eta_0$  is indicated as a viscosity of CT-DNA without metal complexes. Viscosity values of complexes were calculated after correcting the flow time of buffer alone ( $t_0$ ),  $\eta = (t - t_0)/t_0$ .

**DNA damage studies:** The extent of pUC19 DNA cleavage in the presence of an activator  $H_2O_2$  as an oxidizing agent was monitored by using agarose gel electrophoresis [31]. In reaction super coiled pUC19 plasmid DNA Form I (1  $\mu\text{g}$ ) in DMSO (1 %, 2  $\mu\text{L}$ ) was treated with metal complexes (250  $\mu\text{g}$ ) and oxidizing agent  $H_2O_2$  (40 mmol, 5  $\mu\text{L}$ ). The samples were incubated at 1 h at 310 K. A loading of buffer containing bromophenol blue (0.25 %), glycerol (30 %) and xylene cyanol (0.25 %) was added to a platform fixed with a comb to form slots. The electrophoresis was performed at 50 V for 1 h in tris-boric acid-EDTA buffer using 1 % agarose gel containing 0.5  $\mu\text{g}/\text{mL}$  ethidium bromide. The effectiveness of the metal complexes was measured by determining the capacity of complexes converting the super coiled form of DNA to circular form and finally linear form. It was visualized by UV light to photograph the bands.

**Antimicrobial assay:** Minimum inhibitory concentration (MIC) is the very low concentration of an antimicrobial compound that will retard the visible growth of microorganisms at 310 K after overnight incubation. Minimum inhibitory concentrations are important in diagnostic laboratories to confirm the resistance of microorganisms to antimicrobial agents and also

to monitor the activity of new antimicrobial agents. The MIC value of the ligand and its metal complexes were tested against bacterial strains (*Staphylococcus aureus*, *Bacillus subtilis*, *Klebsiella pneumonia* and *Salmonella typhi*) and fungi strains (*Aspergillus niger*, *Aspergillus flavus*, *Curvularia lunata* and *Candida albicans*) through a broth dilutions method. The results of antimicrobial activity associated to the standard antibacterial and antifungal strains as ampicillin and nystatin, respectively. These test concentration of ligand and metal complexes were made from 0.01 to 2.5 mg/ml in the sterile walls of microtiter plates and using 50  $\mu$ L of sterile nutrient broth. The MIC values were determined by reading each well at 492 nm in an automated micro plate reader.

**Cytotoxic activity (MTT assay):** A pair of cancer cell lines such as human breast adenocarcinoma (MCF-7), Human Liver Cancer (Hep G2) and non-cancerous cell lines such as HBL-100, established from human breast milk were purchased from National centre for cell science (NCCS) Pune, India. The cell lines were grown in Dulbecco's modified Eagles medium (DMEM) (Himedia, India) containing 10 % fetal bovine serum (FBS) and 1% antibiotic-antimycotic solutions of all the compounds were prepared in cell culture grade DMSO (Himedia). The effect of treatment of compounds on cell viability was determined using tetrazolium dye by 3-(4,5-dimethyl thiazol-2yl)-2,5-diphenyl tetrazolium bromide (MTT) assay as reported earlier [32]. The cytotoxic effect of dimeric complexes of Cu(II), Co(II), Ni(II), Zn(II) against different cell lines was evaluated by MTT assay. Briefly, the cells were seeded in a 96-well plate and kept in CO for attachment and growth for 24 h and then the cells were treated with various concentrations of complex dissolved in DMSO and incubated for 24 h. After incubation, the culture medium was removed and 15 mL of MTT was discarded and DMSO (100 mL/well) was added to solubilize the purple formazan product. The experiment was carried out in triplicates and the medium without complex served as control. The absorbance was measured calorimetrically at 570 nm using an ELISA micro plate reader. The percentage of cell viability was calculated using the following formula:

$$IC_{50} = \frac{\text{OD value of treated cells}}{\text{OD value of untreated cells (control)}} \times 100$$

A graph was plotted with the percentage of cell inhibition *versus* concentration. From this graph  $IC_{50}$  (concentration of compound to kill 50 % of cells) value was calculated.

***in silico* Biological activity of ligand:** The priority of optimizing ADME-TOX properties of potential drug molecules is now extensively identified [33]. *in silico* ADME-TOX properties of synthesized ligand were studied by using VLS3D online software. Huge number of compounds were barred in clinical development because of awful pharmacokinetics properties [34,35]. But along with the help of cheminformatics online software, it is possible to predict ADME-TOX property through reliable admetSAR, Osiris calculator, SMOP, *etc.* In the present study, absorption, distribution, metabolism, excretion and toxicity properties of the synthesized ligand were calculated by using admetSAR.

**Molecular docking:** Molecular docking is one of the most powerful methods in structure-based drug design, due to its

ability to predict the binding-conformation of small molecule ligands to the suitable target binding site. Characterisation of the binding behaviour plays a significant role in the rational design of drugs as well as to clarify the basic biochemical processes. Pa value was given by the PASS online software. The enzyme is responsible for inflammation of protein data bank. To establish the optimized binding modes of synthesized ligand and its complexes against COX-2 molecular docking studies were accomplished using HEX 8.0 software. Hex 8.0 is a molecular docking software and a bilateral molecular graphics programmes for studying the optimized docking [36] mode between COX-2 and synthesized compound. The structure of ligand and its metal complexes was transformed into PDB file format using Pymole software [37]. The structure was optimized before docking.

## RESULTS AND DISCUSSION

Four different dimeric metal(II) complexes were prepared by using the Schiff base ligand and corresponding metal(II) chloride in the ratio of 2:2 in an ethanol medium. In common organic solvents, the ligand is soluble and its metal complexes are freely soluble in DMSO and DMF, but they are insoluble in many other common organic solvents. Both ligand and complexes are stable at room temperature. Analytical and spectral data of these complexes provide the good result to predict the geometry of the complexes and conductivity values of these complexes indicate that they are electrolytic in nature.

**FT-IR analysis:** FT-IR spectra of compounds explore the bonding nature of the organic compounds and functional group determination. The free ligand affirms  $\nu_{C=O}$  stretching frequency at  $1638\text{ cm}^{-1}$  [38], azomethine ( $\text{HC=N}$ ) occurs at  $1586\text{ cm}^{-1}$  and ( $\text{-C-O-C}$ ) furan ring at  $1027\text{ cm}^{-1}$ . These two peaks are relocated to the region of  $1667\text{-}1633$ ,  $598\text{-}1590$  and  $1014\text{-}1008\text{ cm}^{-1}$ , respectively in all the complexes owing to the coordination of carbonyl and azomethine group of the ligand to metal ion. This value is further supported by M-N characteristic peak at  $444\text{-}423$  and M-O band at  $537\text{-}522\text{ cm}^{-1}$  in all the metal complexes [39].

**Electronic spectral analysis:** The electronic spectrum of the Schiff base ligand L shows intense two bands in 272, 293, 318 and 437 nm matched up to  $n \rightarrow \pi^*$  and  $\pi \rightarrow \pi^*$  transitions for the aromatic ring,  $\text{CH=N}$  and  $\text{C=O}$  groups, respectively. However, these four absorption bands are also observed in the electronic spectra of all synthesized complexes with slight shifts to the higher region in wavelength. This shift may be due to the alteration of molecular environment of Schiff base ligand after the chelation with metal ions [40-42]. The electronic spectra of the ligand and its dimeric Co(II) and Zn(II) complexes are shown in Fig. 1.

**$^1\text{H}$  and  $^{13}\text{C}$  NMR spectra:** In  $^1\text{H}$  NMR spectrum of the ligand displays the multiplet at 7.8-6.8 ppm which is associated to the proton in the phenyl ring, and also it exhibits the peaks at 2.4 (s, 3H), 3.1 (s, 3H) and 8.3 ppm (s, 1H) for  $\text{C-CH}_3$ ,  $\text{N-CH}_3$  and  $\text{CH=N}$ , respectively. In complex  $\text{CH=N}$  group exhibits a peak at 9.3 ppm, which indicates the coordination of azomethine group during the complexation with zinc ion [43].

$^{13}\text{C}$  NMR spectrum of Schiff base ligand indicates the carbon environment of phenyl group at 55.2-136.3 ppm. It

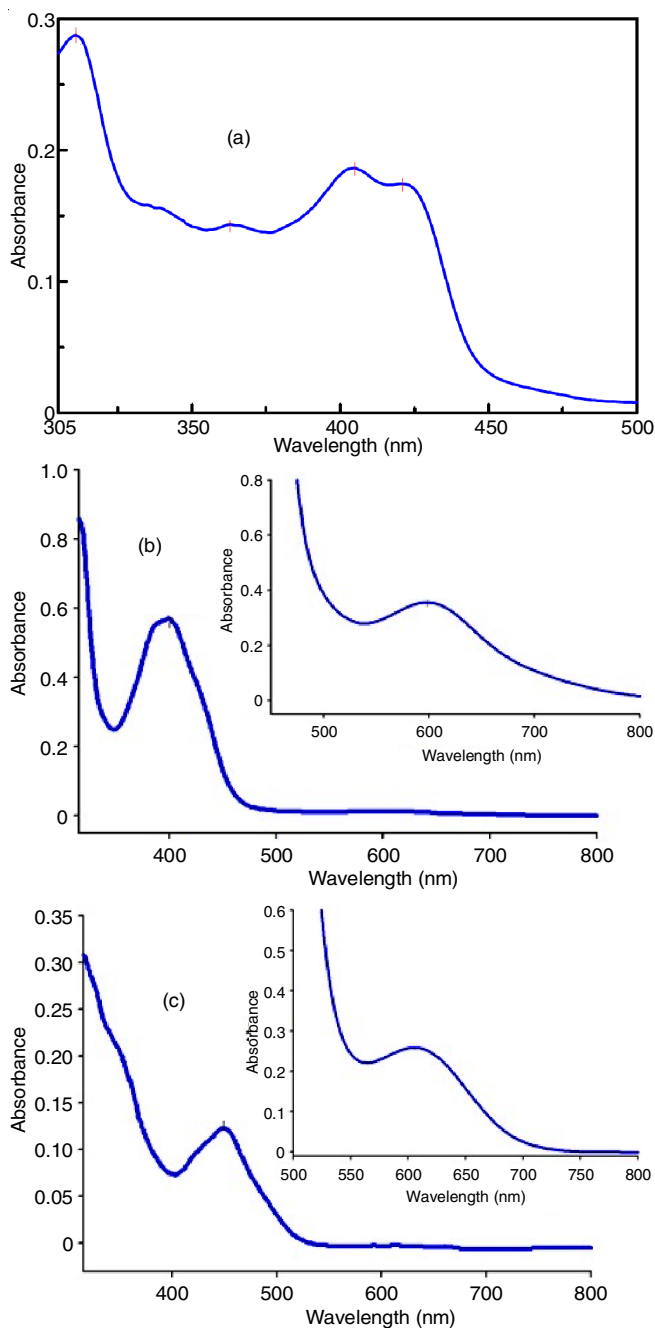


Fig. 1. Electronic spectra of (a) ligand, (b)  $[\text{CoLCl}_2]_2$  and (c)  $[\text{ZnLCl}_2]_2$  complexes

also exhibits C-CH<sub>3</sub>, N-CH<sub>3</sub>, HC=N, C=O and C-O signals at 10.4, 36.8, 161.2, 152.2 and 145.7 ppm, respectively. In dimeric  $[\text{ZnLCl}_2]_2$  complex, HC=N, C=O and C-O groups are shifted to downfield due to coordination of azomethine and carbonyl group containing donor atoms with zinc ion [44]. There is no significant change in all other signals in the synthesized dimeric  $[\text{ZnLCl}_2]_2$  complex.

**Electron spin resonance analysis:** ESR spectroscopy has been considered as the most admirable technique to scrutinize the metal environment in the complexes [45]. It is used to analyze the geometry and nature of bonding between copper ion and its ligand, mainly in dimeric Cu(II) complex. In the present study, ESR spectrum of dimeric  $[\text{CuLCl}_2]_2$  was effectuated. The recorded ESR spectrum of dimeric  $[\text{CuLCl}_2]_2$  is represented in Fig. 2.

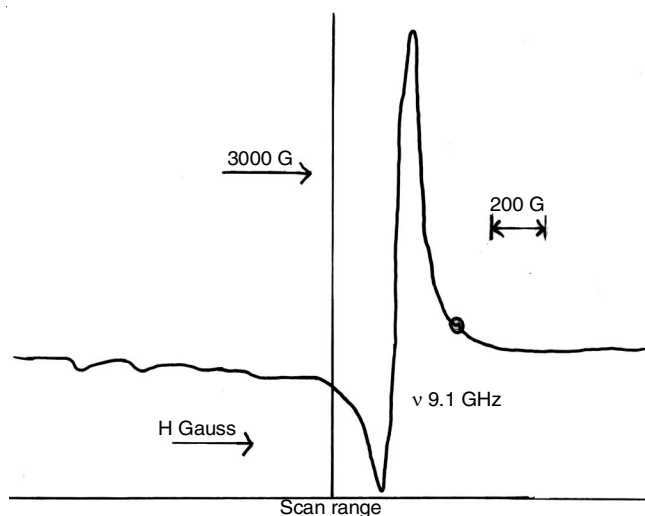


Fig. 2. EPR spectrum of Cu(II) complex in DMSO solution at LNT

It explained two g factors  $g_{\parallel}$  and  $g_{\perp}$ , the calculated spin Hamiltonian spectral data of dimeric  $[\text{CuLCl}_2]_2$  are presented in Table-1. From this spectral data, it is found that  $g_{\parallel}$  (2.24) >  $g_{\perp}$  (2.03) >  $g_e$  (2.0024), which revealed that the one unpaired electron is present in ( $d_{x^2-y^2}$ ) orbital and it is likely to be the octahedral geometry as conferred in electronic spectroscopy [46]. The  $g_{\parallel}$  value of dimeric Cu(II) complex can be used as a measure of covalent behaviour of copper-ligand interaction. If the value is higher than 2.4, copper-ligand bond is basically ionic and the value less than the 2.4 is symptomatic of covalent character. In the present ESR results, lesser value of  $g_{\parallel}$  (2.24) is correlated to 2.4 which is an excellent substantiation for the covalent character of Cu-nitrogen interactions, as recommended by Kivelson and Neiman [47]. From the values of g factors, the exchange coupling factor (G) can be expressed by the following equation:

$$G = \frac{g_{\parallel} - 2}{g_{\perp} - 2}$$

It has been already investigated that if  $G > 4.0$ , the local tetragonal axes are aligned parallel or slightly misaligned. If  $G < 4.0$ , considerable exchange coupling might be present and generate the considerable misalignment. In this study, the observed G value of  $[\text{CuLCl}_2]_2$  is 5.4 which explains that the local tetragonal axes are aligned parallel or slightly misaligned and exchange coupling could be worthless [48]. The observed empirical ratio of  $g_{\parallel}/A_{\parallel}$  value for the dimeric complex  $[\text{CuLCl}_2]_2$  is 162 which pointed out the octahedral geometry of dimeric  $[\text{CuLCl}_2]_2$  with small distortion.

**ESI-MS spectrum:** Peaks conducted from mass spectra of the ligand and its dimeric Cu(II), Co(II), Ni(II) and Zn(II) complexes was attributed to the molecular ions  $m/z$  at 281, 831.5, 822.3, 821.8  $M^+$  and 835.2  $M^+$ , respectively. This fact was matched to the suggested molecular formula for these synthesized compounds *i.e.* ligand,  $[\text{CuLCl}_2]_2$ ,  $[\text{CoLCl}_2]_2$ ,  $[\text{NiLCl}_2]_2$  and  $[\text{ZnLCl}_2]_2$ , where L = 4-(furan-2-ylmethyleneamino)-1,5-dimethyl-2-phenyl-1,2-dihydro-3H-pyrazol-3-one. This confirms the Schiff-base frame formation. Elemental analysis values were appropriate with those values calculated from the molecular formulae assigned to these complexes which are further supported by mass studies.

TABLE-1  
THE SPIN HAMILTONIAN PARAMETERS OF Cu(II) COMPLEX IN DMSO SOLUTION AT LNT

Complex	g-Tensor			$A \times 10^{-4} (\text{cm}^{-1})$			
	$g_{\parallel}$	$G_{\perp}$	$g_{\text{iso}}$	$A_{\parallel}$	$A_{\perp}$	$A_{\text{iso}}$	G
Cu(II)	2.24	2.03	2.0024	134	69	83	5.4

**XRD, EDX, SEM and TEM morphological studies:** In Fig. 3, XRD patterns of  $[\text{CuLCl}_2]_2$ ,  $[\text{CoLCl}_2]_2$ ,  $[\text{NiLCl}_2]_2$  and  $[\text{ZnLCl}_2]_2$  complexes are given. The indexing procedures were performed using (CCP4, UK) CRYSFIRE program [49,50] giving triclinic crystal system for  $[\text{CuLCl}_2]_2$  having  $M(9) = 8$ ,  $F(6) = 7$ ,  $[\text{CoLCl}_2]_2$  monoclinic crystal system having  $M(9) = 8$ ,  $F(6) = 9$ , orthorhombic crystal system for  $[\text{NiLCl}_2]_2$  having  $M(6) = 15$ ,  $F(6) = 5$ , and monoclinic crystal system for  $[\text{CuLCl}_2]_2$  having  $M(6) = 7$ ,  $F(6) = 11$  as the superior solutions. Their cell parameters are interpreted in Table-2.

The SEM images of  $[\text{CuLCl}_2]_2$ ,  $[\text{CoLCl}_2]_2$ ,  $[\text{NiLCl}_2]_2$  and  $[\text{ZnLCl}_2]_2$  complexes are shown in Fig. 4a-d, respectively. The micrograph of  $[\text{CuL}_2] \cdot 2\text{Cl}$  complex shows peel shaped particles. The  $[\text{CoLCl}_2]_2$  and  $[\text{ZnLCl}_2]_2$  complexes mention ice rock structure. The  $[\text{NiLCl}_2]_2$  and  $[\text{ZnLCl}_2]_2$  complexes grain-structure of ice was existent. The results by EDX analysis explained that copper, cobalt, nickel, zinc and carbon, nitrogen and oxygen peaks, which meant there were copper, cobalt, nickel, zinc and carbon, nitrogen and oxygen deposited products as shown in Fig. 5a-d. The EDX line traces indicate that  $[\text{CuLCl}_2]_2$ ,  $[\text{CoLCl}_2]_2$ ,  $[\text{NiLCl}_2]_2$

and  $[\text{ZnLCl}_2]_2$  they have been successfully integrated into the sample structure. All positions contain predictable elements, and different elements such as impurity were not detected.

Fig. 6a-c shows the TEM images of  $[\text{CuLCl}_2]_2$ ,  $[\text{CoLCl}_2]_2$ ,  $[\text{NiLCl}_2]_2$  and  $[\text{ZnLCl}_2]_2$  complexes, respectively. The consistency and resemblance in between the particle forms of synthesized dimeric complexes, suggest that the structural phases have a similar template. The particles diameter is found in the nano-range as follow: Cu(II), 57-228 nm; Co(II), 43-173 nm; Ni(II), 18-23 nm and Zn(II), 12-32 nm. Nanoparticle-size complexes may act strong in different application areas between a biological one. Complexation feature is also authenticated from the SEM image of the respective dimeric complex  $[\text{Cu(II)}$ , Co(II), Ni(II), Zn(II)] has the different features with smooth and rough surface regions. It is also further evidenced by the brighter region, which indicates the presence of metallic species in the samples and thus confirming the presence of dimeric Cu(II), Co(II), Ni(II) and Zn(II) ions in the synthesized compound.

**Thermal analysis:** Thermal decomposition of dimeric complexes (1-4), was studied in the temperature range 30-1200 °C.

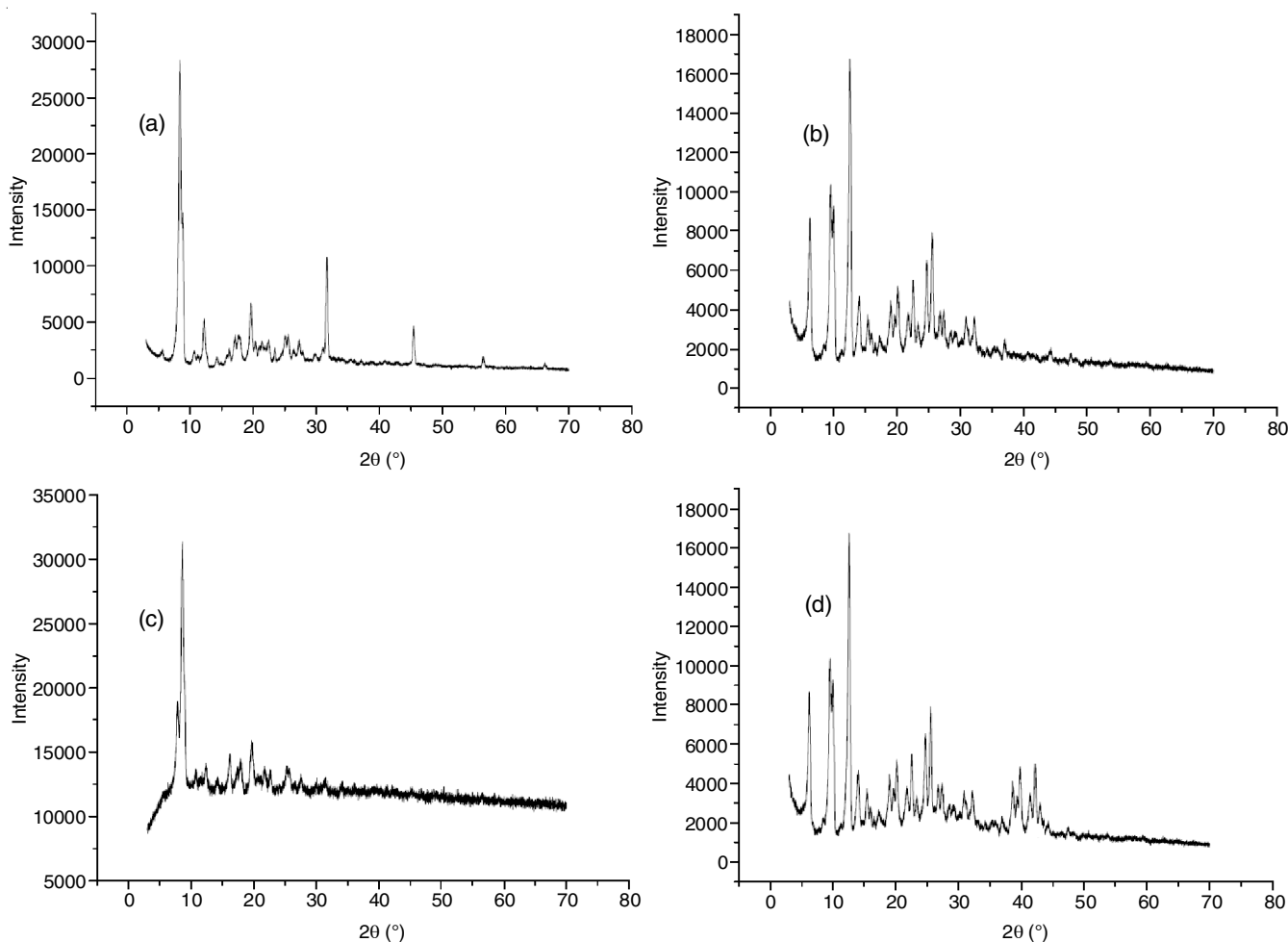


Fig. 3. Powder XRD spectra of (a)  $[\text{CuLCl}_2]_2$ , (b)  $[\text{CoLCl}_2]_2$ , (c)  $[\text{NiLCl}_2]_2$  and (d)  $[\text{ZnLCl}_2]_2$  complexes, respectively

TABLE-2  
CRYSTALLOGRAPHIC DATA FOR THE SCHIFF BASE COMPLEXES  $[\text{CuLCl}_2]_2$ ,  $[\text{CoLCl}_2]_2$ ,  $[\text{NiLCl}_2]_2$  AND  $[\text{ZnLCl}_2]_2$

Data	$[\text{CuLCl}_2]_2$	$[\text{CoLCl}_2]_2$	$[\text{NiLCl}_2]_2$	$[\text{ZnLCl}_2]_2$
Empirical formula	$\text{CuC}_{32}\text{H}_{30}\text{N}_6\text{O}_4\text{Cl}_2$	$\text{CoC}_{32}\text{H}_{30}\text{N}_6\text{O}_4\text{Cl}_2$	$\text{NiC}_{32}\text{H}_{30}\text{N}_6\text{O}_4\text{Cl}_2$	$\text{ZnC}_{32}\text{H}_{30}\text{N}_6\text{O}_4\text{Cl}_2$
Formula weight (g/mol)	831.5	822.3	821.8	835.2
Wavelength (Å)	0.71073	0.71073	1.54056	1.54056
Crystal system	Triclinic	Monoclinic	Orthorhombic	Monoclinic
Space group	P?	Pn	Pbca	Pn
a (Å)	5.8596(3)	9.0086(7)	12.287 (5)	8.9981(5)
b (Å)	9.6932(5)	19.1090(13)	11.884 (5)	12.6314(8)
c (Å)	12.8257(7)	18.589(2)	37.152 (5)	19.4346(10)
$\alpha$ (°)	116.649(6)	90	90	90
$\beta$ (°)	92.899(5)	101.46(3)	90	103.019(4)
$\gamma$ (°)	102.230(5)	90	90	90
Volume (Å <sup>3</sup> )	3325.7(4)	854.36(4)	5854.3(4)	856.46(4)
(Calc.) density (g/cm <sup>-3</sup> )	1.358	1.989	1.543	1.993
2 $\theta$ range	1.71–28.27	1.71–28.27	10.25–67.27	12.56–68.00
Limiting indices	$-16 \leq h \leq 6$ $-15 \leq k \leq 5$ $-15 \leq l \leq 5$	$-6 \leq h \leq 7$ $-34 \leq k \leq 34$ $-12 \leq l \leq 9$	$0 \leq h \leq 15$ $0 \leq k \leq 15$ $0 \leq l \leq 47$	$-10 \leq h \leq 10$ $-12 \leq k \leq 12$ $-25 \leq l \leq 25$
Z	2	4	8	2
R <sub>f</sub>	0.0000842	0.000847	0.0000323	0.0000907
Temperature (K)	298	298	298	298

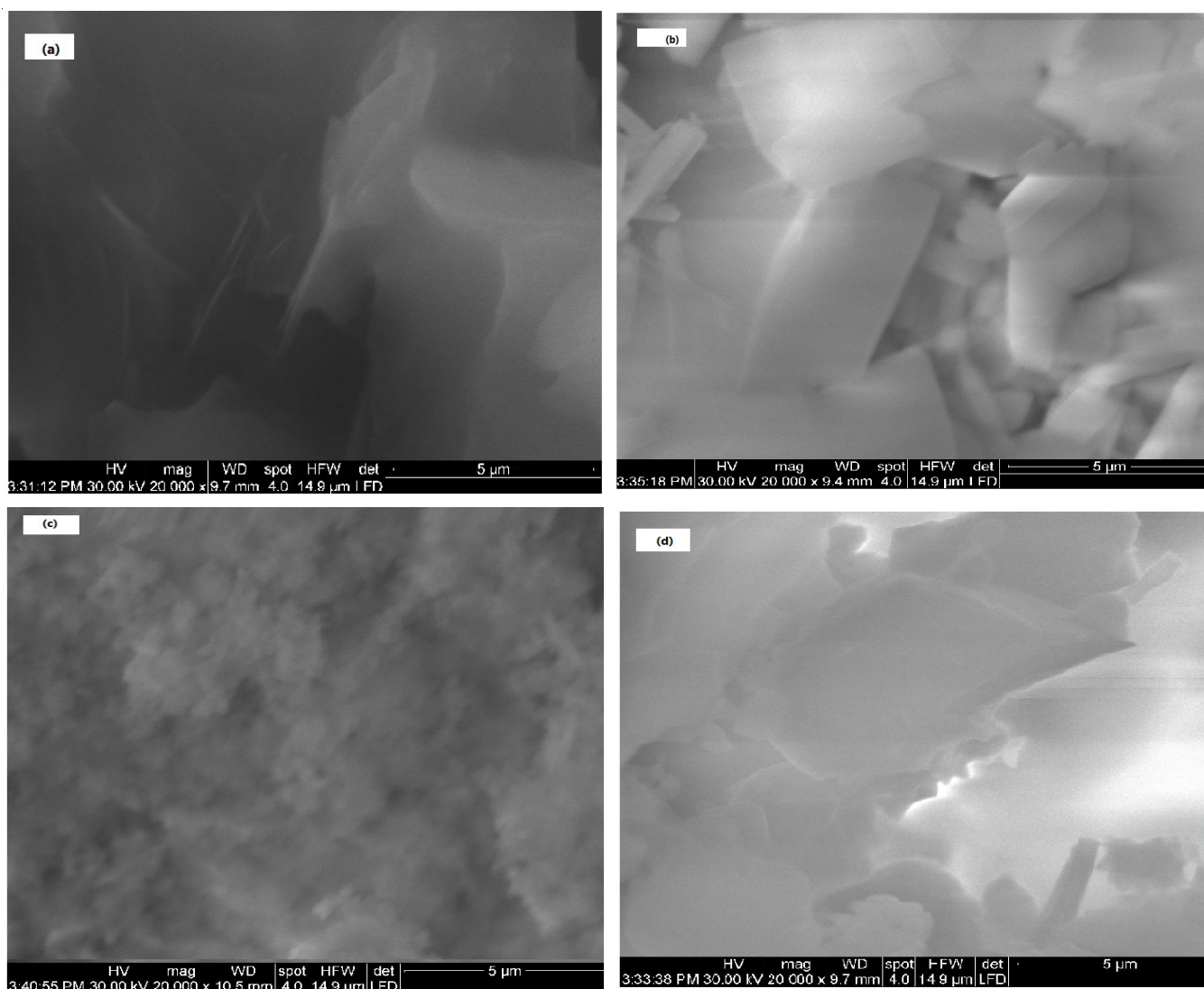


Fig. 4. SEM images of (a)  $[\text{CuLCl}_2]_2$ , (b)  $[\text{CoLCl}_2]_2$ , (c)  $[\text{NiLCl}_2]_2$  and (d)  $[\text{ZnLCl}_2]_2$  complexes

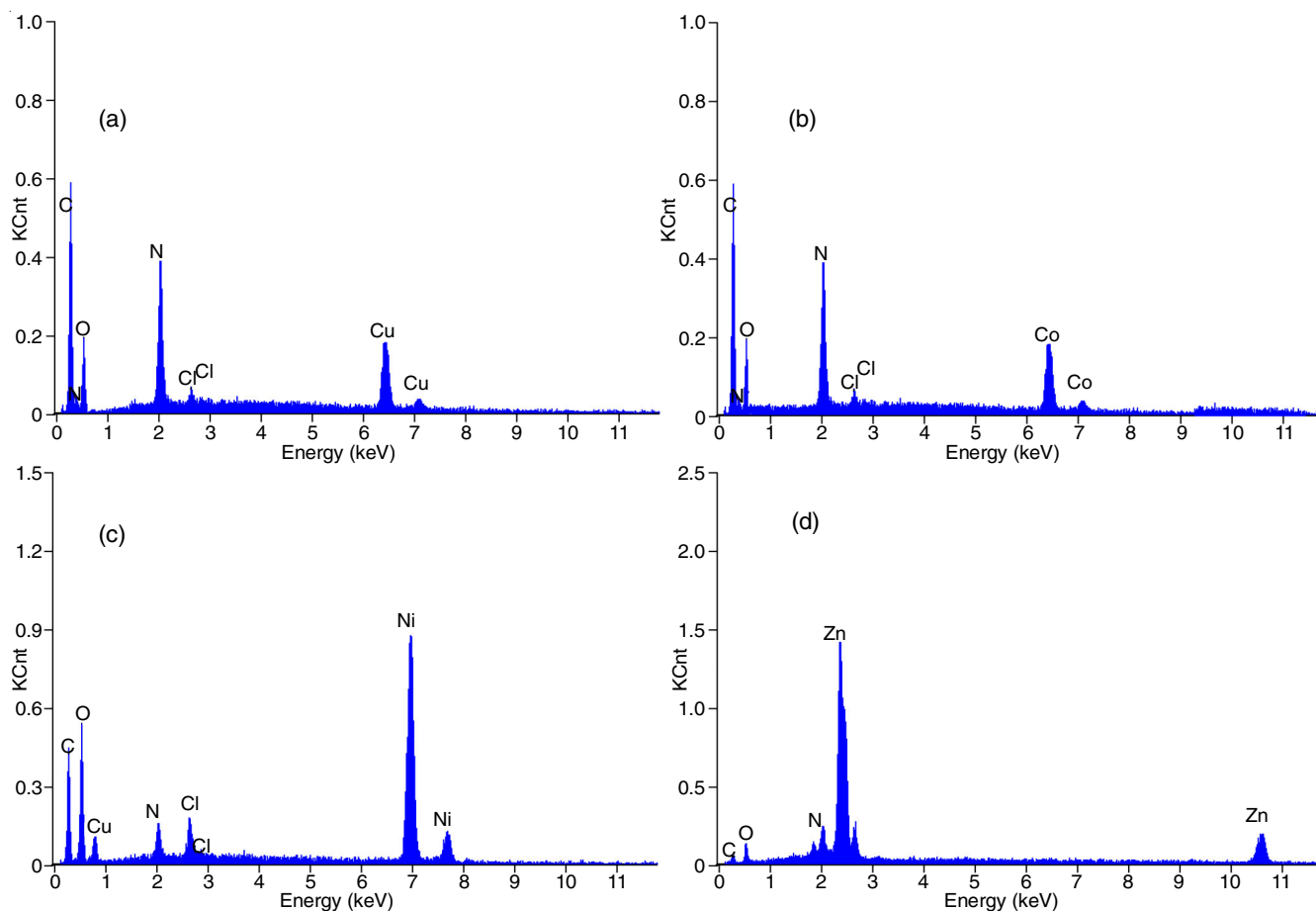


Fig. 5. EDX images of (a)  $[\text{CuLCl}_2]_2$ , (b)  $[\text{CoLCl}_2]_2$ , (c)  $[\text{NiLCl}_2]_2$  and (d)  $[\text{ZnLCl}_2]_2$  complexes, respectively

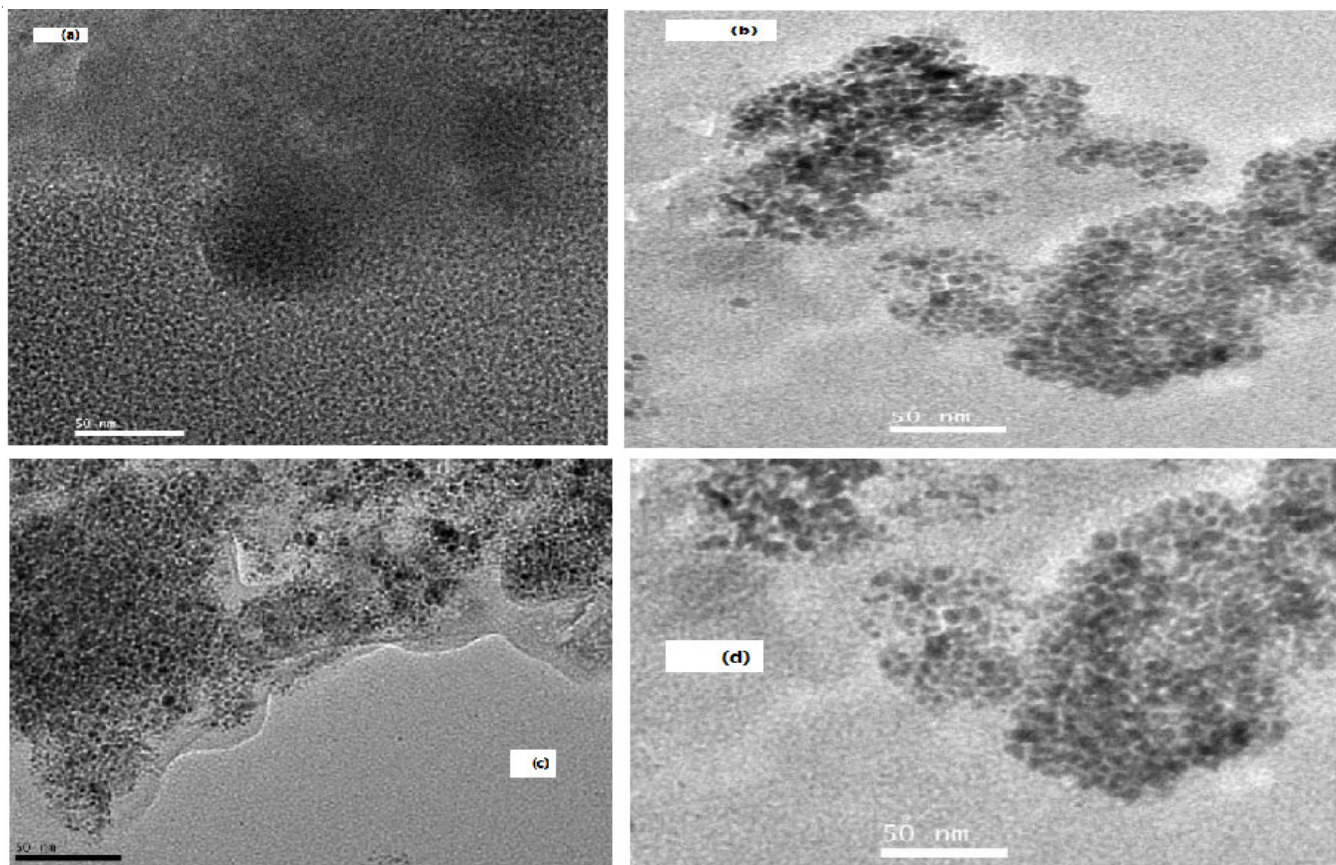


Fig. 6. TEM images of (a)  $[\text{CuLCl}_2]_2$ , (b)  $[\text{CoLCl}_2]_2$ , (c)  $[\text{NiLCl}_2]_2$  and (d)  $[\text{ZnLCl}_2]_2$  complexes

All the thermogravimetric analysis curves for dimeric complexes (1-4) are shown in Fig. 7. No change in weight was observed in the range 90-268 °C, which indicated the absence of coordinated or uncoordinated water. During the experiment, all the dimeric complexes first underwent a decomposition step and exhibited a decrease of 7.18-14.76 % (7.24-14.89 %) in weight in the range 265-270 °C owing to the removal of chloride anions. The complexes underwent a second decomposition step 79.32-81.59 % (79.38-81.62 %) in the temperature range 380-1100 °C due to the loss of complete ligand. IR spectroscopy was used to analyze and identify the final residue as metal oxide corresponding to calculated value.

**Kinetic studies:** Graphical estimation methods, such as Coats-Redfern [51], Horowitz-Metzger [52] and Piloyan-Novikova [53] methods, were used to determine the kinetic parameters (Table-3) such as thermal activation energy of decomposition ( $E_a$ ), enthalpy ( $\Delta H^\ddagger$ ), entropy ( $\Delta S^\ddagger$ ) and Gibbs free energy change of decomposition ( $\Delta G^\ddagger$ ) of the complexes. The following conclusions were drawn from the results obtained:

- The high values of the energy of activation,  $E_a$  of the complexes indicated that the metal complexes were highly stable owing to their covalent bond character.

- The complexes that were analyzed exhibited positive  $\Delta G$  values, thus indicating that the free energy of final residue was higher than that of initial compounds; hence, the complexes underwent decomposition non-spontaneously. Furthermore, the values of activation ( $\Delta G$ ), increased significantly in the subsequent decomposition stages of a given complex. This observation can be explained by the significant increase in the values of  $T\Delta S$  from one step to the next, which predominated the values of  $\Delta H$ .

- The negative values of  $\Delta S$  for the decomposition steps indicated that all the studied dimeric complexes were more ordered in their activated states than in their resting states.

**Antimicrobial screening:** The *in vitro* antimicrobial activities of synthesized Schiff base ligand (L) and its corresponding dimeric metal(II) complexes were tested using cultures of *Staphylococcus*

*aureus* (gram-positive bacterium), *Bacillus subtilis* (gram-positive bacterium), *Salmonella typhi* and *Escherichia coli* (both gram-negative bacterium) as well as those of fungi, such as *Aspergillus niger*, *Aspergillus flavus*, *Curvularia lunata* and *Candida albicans*, by using the broth micro dilution method. Ampicillin and nystatin were used as standard drugs for antibacterial and antifungal activity studies, respectively. The results of antimicrobial activity studies with the Schiff base and its metal complexes are presented in Table-4. The dimeric metal(II) complexes showed higher antimicrobial activities than did L. These observations can be explained by Overton's concept and Tweedy's chelation theory [54]. According to this concept, chelation considerably reduces the polarity of metal ions because of partial donation of positive charges to the donor groups and  $\pi$ -electron delocalization within the entire chelating ring system. The reduction in polarity of the metal ion increased the lipophilicity of complexes and enhanced the interaction between the metal ion and lipid bilayer, thus facilitating the diffusion of (chelated) metal ion through the cell membrane. The minimum inhibitory concentration values of the complexes indicated that the activity of the complexes against the selected bacteria and fungi stains was higher than that of ligand because of the presence of azomethine (HC=N) group in ligand and its chelating effect on the central metal ion. The azomethine group and its chelating effect improved the efficiency of antibacterial agents, and the metal complexes exhibited either microbicidal or microbiostatic effects by blocking the active sites of crucial enzymes [55]. In addition, the main ligand containing (oxygen and nitrogen) donor groups might reduce enzyme activity. Because the enzymes need the groups (donor atoms) for their activity, they are highly susceptible to deactivation by the metal ion because of chelation.

***in vitro* Cytotoxicity assay:** The *in vitro* antiproliferative activity was assayed using two cancer cell lines, namely (MCF-7) (human breast adenocarcinoma cancer cell line), Hep G2 (human liver carcinoma cell line) and HBL-100, which is a non-cancerous cell line established from human breast milk), through

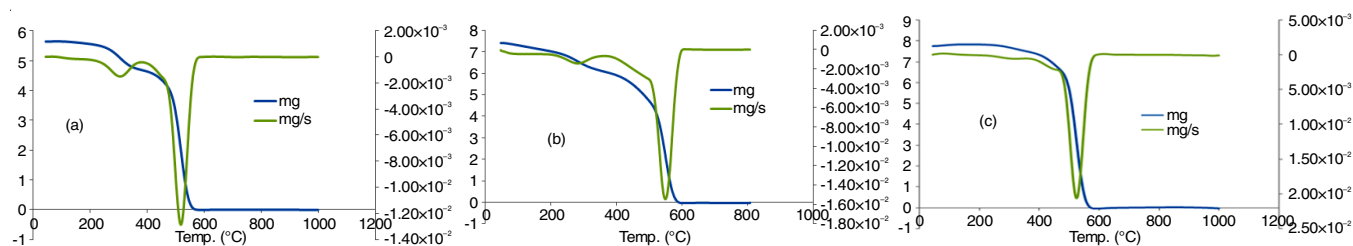


Fig. 7. TG/DTG of (a) Cu(II), (b) Co(II), and (c) Ni(II) complexes respectively up to 1000 °C

TABLE-3  
KINETIC PARAMETERS OF Cu(II), Co(II) AND Ni(II) COMPLEXES

Compound	Decomposition temp. (°C)	Method	Parameters					Correlation coefficient
			$E_a$ (kJ mol <sup>-1</sup> )	A (s <sup>-1</sup> )	$\Delta S^\ddagger$ (J mol <sup>-1</sup> K <sup>-1</sup> )	$\Delta H^\ddagger$ (kJ mol <sup>-1</sup> )	$\Delta G^\ddagger$ (kJ mol <sup>-1</sup> )	
[CuLCl <sub>2</sub> ] <sub>2</sub>	142–372	CR	38.9	162	-203	54.2	162	0.9924
		HM	42.3	163	-207	55.6	165	0.9928
		PN	41.7	162	-205	56.0	163	0.9929
[CoLCl <sub>2</sub> ] <sub>2</sub>	193–347	CR	68.8	180	-238	54.2	167	0.9896
		HM	68.3	182	-236	64.8	166	0.9899
		PN	69.1	179	-237	65.2	164	0.9897
[NiLCl <sub>2</sub> ] <sub>2</sub>	187–374	CR	66.6	169	-242	64.7	159	0.9887
		HM	67.2	170	-244	55.8	158	0.9888
		PN	66.8	171	-243	56.3	157	0.9885

TABLE-4  
MINIMUM INHIBITORY CONCENTRATION OF THE SYNTHESIZED FREE LIGAND  
AND ITS METAL COMPLEXES AGAINST THE GROWTH OF BACTERIA AND FUNGI (?M)

Compound	Bacteria: MIC values ( $\times 10^4 \mu\text{M}$ ) SEM = $\pm 1.5$				Fungi: MIC values ( $\times 10^4 \mu\text{M}$ ) SEM = $\pm 1.3$			
	<i>S. aureus</i>	<i>B. subtilis</i>	<i>S. typhi</i>	<i>E. coli</i>	<i>A. niger</i>	<i>A. flavus</i>	<i>C. lunata</i>	<i>C. albicans</i>
Ligand	24.5	25.8	27.5	24.9	26.8	25.3	25.8	25.7
Cu(II)	9.6	92	10.4	10.5	11.3	11.3	12.4	12.7
Co(II)	11.8	10.8	11.4	11.6	13.5	13.9	11.6	12.7
Ni(II)	10.1	11.6	9.7	10.8	12.7	12.8	13.9	13.5
Zn(II)	9.8	10.4	9.4	9.7	11.9	12.5	11.2	11.6
Ampicillin	2.6	3.2	4.2	4.4	–	–	–	–
Nystatin	–	–	–	–	3.5	3.8	4.3	4.8

the MTT assay by using cisplatin as a standard (positive control). The principle of MTT assay is that only viable cells can reduce yellow MTT to form purple formazan products, whereas non-viable cells cannot. Therefore, the metabolic activities of cells were evaluated using their capability to cleave the tetrazolium rings of yellow MTT and produce the purple formazan crystals. The MTT assay results showed that the metal complexes hindered the growth of cancer cells. The above-mentioned cell lines were treated with the synthesized metal complexes at different concentrations (0-100 mM) for 48 h. The results of cell inhibition were expressed as IC<sub>50</sub> values. These values are listed in Table-5 and cell viability depended on the concentration of dimeric metal(II) complexes. The IC<sub>50</sub> values decreased with an increase in the concentration of dimeric metal(II) complexes, which indicated that the cytotoxicity effect of synthesized dimeric complexes depended on the dose and duration of exposure. All the dimeric Cu(II), Co(II), Ni(II) and Zn(II) complexes showed remarkable cytotoxicity toward the cancer cell lines, (MCF-7) and HepG2. Among these complexes, copper complex caused the highest growth hindrance in the MCF-7 and HepG2 under the similar experimental conditions. The high cytotoxic effect of copper complex may be associated with the size, charge (on metal ion), ionic radius, primary ligand, steric and pharmacokinetic factors, which collectively play a prominent role in the potency of the drugs [56]. The IC<sub>50</sub> values of complex in MCF-7 and HepG2 cell lines were 14 and 19 mM, respectively. In particular, *in vitro* antiproliferative activity testing of the synthesized compounds against non-cancerous cell line HBL-100 showed that IC<sub>50</sub> value was > 87  $\mu\text{M}$ . This indicated that all the dimeric complexes behave differently toward cancer cells and non-cancerous cells and are less toxic to the HBL-100 cells than to the cancerous cells. Thus, the IC<sub>50</sub> values are inversely proportional to the biological potential of the compound.

TABLE-5  
CYTOTOXICITY OF Cu(II), Co(II), Ni(II), Zn(II) COMPLEXES  
AGAINST MCF-7, HepG2 AND HBL-100 HUMAN CELL LINES

Complexes	IC <sub>50</sub> values (mM)		
	MCF-7	HepG 2	HBL-100
Cu(II)	14 $\pm$ 0.9	19 $\pm$ 0.9	82 $\pm$ 0.9
Co(II)	28 $\pm$ 1.2	28 $\pm$ 1.2	95 $\pm$ 1.0
Ni(II)	24 $\pm$ 0.7	22 $\pm$ 1.2	91 $\pm$ 0.5
Zn(II)	20 $\pm$ 0.6	25 $\pm$ 0.7	87 $\pm$ 0.7
Cisplatin (standard)	17 $\pm$ 1.2	21 $\pm$ 1.2	85 $\pm$ 1.1

**Molecular docking analysis:** Molecular docking is a meticulous method to investigate the drug-nucleic acid interactions

for the blooming of modern drug design and findings as well as to discover the exact binding site offered at the molecular target DNA, mostly in a non-covalent interaction [57]. The probable binding modes of the synthesized ligand and dimeric metal(II) complexes were prearranged in HEX 8.0 software against COX-2 (cyclooxygenase) receptor molecule which is based on PASS biological activity prediction score. COX-2 enzyme is an inflammation response, which was recovered from PDB database (Protein Data Bank) (PDB ID:1CX2). It is universally acknowledged that if the binding free energy is low, then the binding affinity is more effective in between the receptor (DNA) and "ligand" (Schiff base and its dimeric metal(II) complexes) molecules, for the reasons, molecular docked model poses are depicted in Fig. 8, which evidently explicates that Schiff base ligand and its metal complexes with DNA through an intercalation mode concerning outside edge stacking contact with the oxygen atom of the phosphate backbone, it is clear that the ligand and dimeric metal(II) complexes were to be positioned suitably into the intercalation mode of targeted DNA. In addition, resultant structures are stabilized by the vander Waal's interaction and hydrophobic contacts with DNA functional group that delineate the stability of interaction [58]. The docking scores of molecular docked ligand and the dimeric metal(II) complexes (Cu<sup>2+</sup>, Co<sup>2+</sup>, Ni<sup>2+</sup>, Zn<sup>2+</sup>) are found to be (-253.4), (-289.7), (-289.5), (-289.3), (-289.2), respectively. It is very enthralling to note that the binding energy of [CuL<sub>2</sub>].2Cl is higher than that of other complexes and the order of binding energy is as follows [CuLCl<sub>2</sub>]<sub>2</sub> > [CoLCl<sub>2</sub>]<sub>2</sub> > [NiLCl<sub>2</sub>]<sub>2</sub> > [ZnLCl<sub>2</sub>]<sub>2</sub>. These data suggested that the dimeric metal(II) complexes have more medicinal power and intended to reduce the inflammation or swelling (due to heat and chemicals) than ligand.

#### DNA Interaction studies

**Electronic absorption titration:** The UV-visible spectra of [CuLCl<sub>2</sub>]<sub>2</sub> and [ZnLCl<sub>2</sub>]<sub>2</sub> complexes in the presence or absence of CT-DNA are given in Figs. 9 and 10. DNA binding effects of metal complexes possess powerful authentication for the growth of efficient metal based chemotherapeutic drugs. The absorption spectral titration is a most credible instrument for observing the metal-DNA interacting mechanism and complex formation. The transition and inner transition metal complexes bind to DNA through the covalent or non-covalent and electrostatic binding interactions [59]. These binding propensities of [CuLCl<sub>2</sub>]<sub>2</sub>, [CoLCl<sub>2</sub>]<sub>2</sub>, [NiLCl<sub>2</sub>]<sub>2</sub> and [ZnLCl<sub>2</sub>]<sub>2</sub> complexes are achieved by the diverse methods. One of the most important method is electronic absorption titration. The deformation of DNA structure is frequently correlated with the anticancer activity.

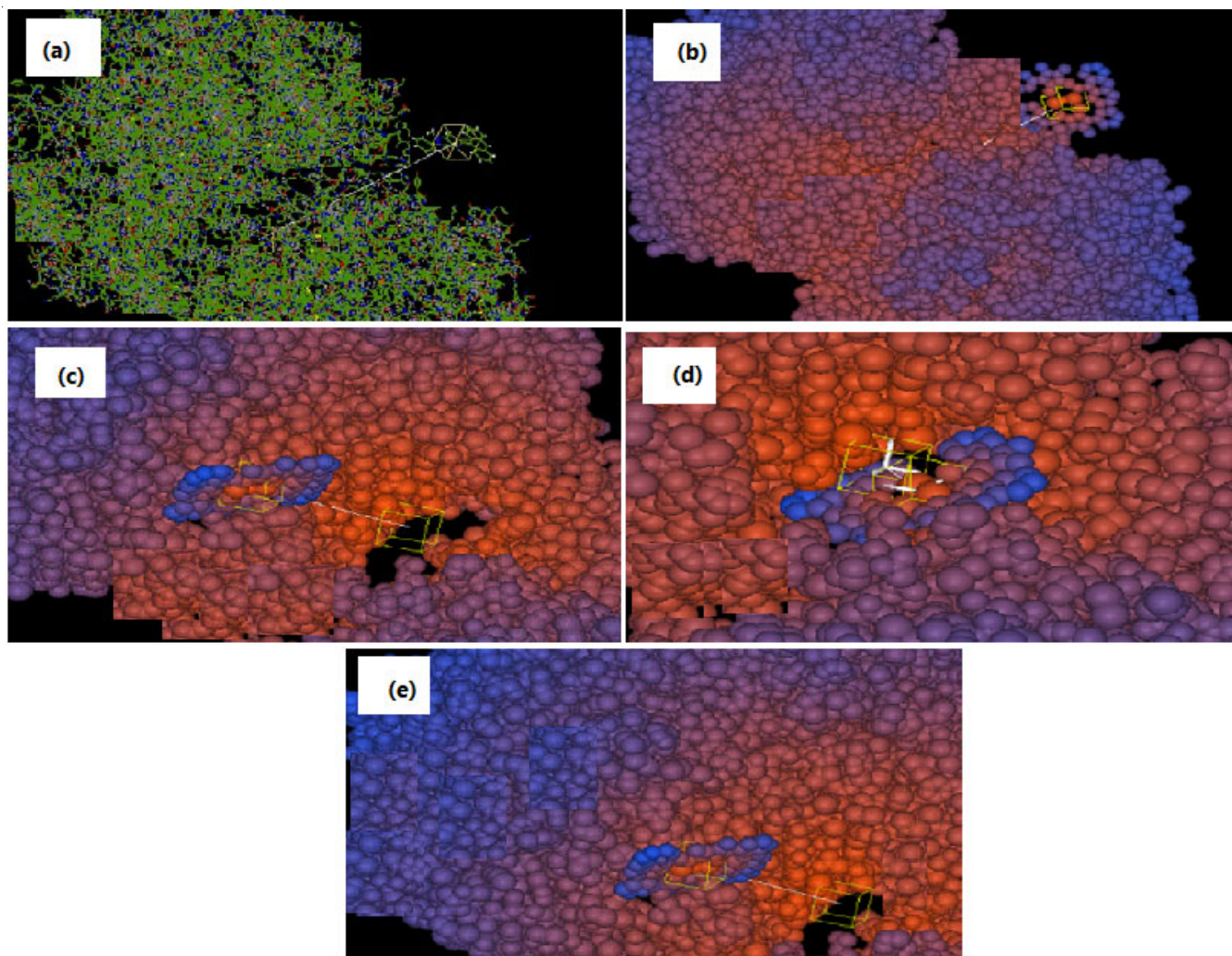


Fig. 8. Binding model of synthesized compound with COX-2 receptor: (a) Schiff base ligand; (b) Cu(II), (c) Co(II), (d) Ni(II) and (e) Zn(II) complexes

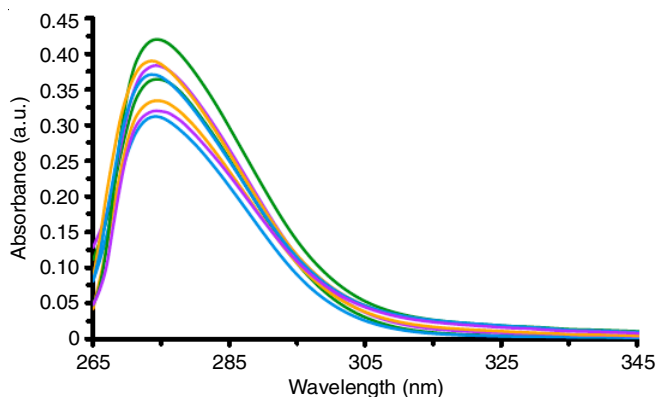


Fig. 9. Electronic absorption spectra of  $[\text{CuLCl}_2]_2$  in 5 mM Tris-HCl/50 mM NaCl buffer (pH = 7.2 at 298 K) in the presence of increasing amount of CT-DNA

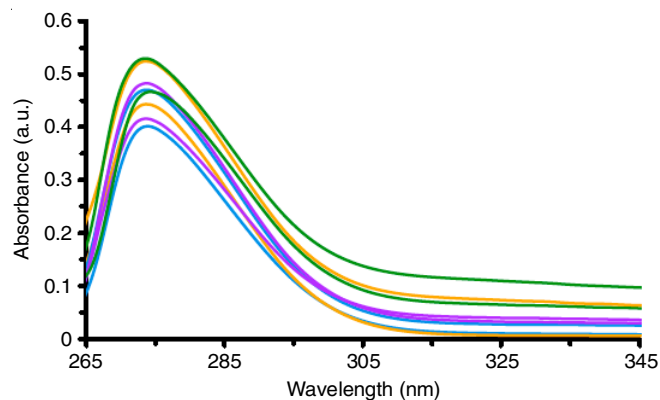


Fig. 10. Electronic absorption spectra of  $[\text{ZnLCl}_2]_2$  in 5 mM Tris-HCl/50 mM NaCl buffer (pH = 7.2 at 298 K) in the presence of increasing amount of CT-DNA

Therefore, to conclude the anticancer mediator, DNA binding study is considered as an essential one. In this binding study, the above-mentioned metal complexes were recorded by using 5 mM tris-HCl/50 mM NaCl buffer solution (pH = 7.2). The absorption spectra of all the complexes indicated an intensive absorption band in the region around 336-346 nm, in 5mM tris-HCl/50 mM NaCl (pH 7.2) buffer solution. At a fixed concen-

tration of the complexes they were titrated with increasing amount of CT-DNA (each addition of 30  $\mu\text{L}$ ). The increasing amount of CT-DNA results from hypsochromic shift in the range of 3-5 nm and significant hypochromicity [60]. The observed hypochromism might to be accredited for the stacking interactions between DNA and aromatic chromophore of dimeric complexes, which are consistent with all the dimeric metal(II) complexes

binding to CT-DNA through the intercalative binding mode and the absorbed hypochromicity ( $H\%$ ) of these synthesized dimeric complexes exhibits  $\sim 11-17\%$  which clearly denotes that all the dimeric metal(II) complexes strongly bind to DNA. The intrinsic binding constant values of  $K_b$ , were calculated from the slope by intercept values obtained from the plots between  $[DNA]/(\epsilon_b - \epsilon_f)$  and  $[DNA]$  which are given in Table-6.

TABLE-6  
ELECTRONIC ABSORPTION PARAMETERS  
FOR THE INTERACTION OF DNA WITH Cu(II),  
Co(II), Ni(II) AND Zn(II) COMPLEXES  
 $^aH(\%) = [(A_{\text{free}} - A_{\text{bound}})/A_{\text{free}}] \times 100$

Complexes	$\lambda_{\text{max}}$		$\Delta\lambda$ (nm)	$^aH$ (%)	$K_b \times 10^4$ ( $M^{-1}$ )
	Free	Bound			
Cu(II)	336	342	5	16.9	9.7
Co(II)	337	342	4	14.6	7.4
Ni(II)	338	343	4	11.8	5.7
Zn(II)	346	350	3	11.2	6.3

**Viscosity measurements:** The DNA-binding action of the complex was determined using viscometric measurement. This method is considered as the least ambiguous and most crucial test for the DNA binding in solution. The viscosities were performed at room temperature. Partial and non-classical intercalative compounds can bend or kick the DNA, thus reducing its effective length and minimizing the viscosity of the DNA. This measurement provides the evidence to support the occurrence of intercalative binding. Furthermore, viscometry is the useful tool for determining the changes in the length of DNA and providing information about the binding mode of dimeric metal(II) complexes with DNA. An increase in the viscosity was observed owing to the intercalative binding in DNA because the intercalation between the base pairs causes lengthening of DNA polymer due to effective DNA base pairs separation. Ethidium bromide is commonly used as a strong intercalating agent in DNA-binding studies, because it can be easily accommodated in between the DNA base pairs, which is expected to lengthen the DNA double helix. The explicit viscosities of DNA plotted against  $[\text{complex}]/[\text{DNA}]$  versus  $\eta/\eta_0^{1/3}$ , are shown in Fig. 11, where  $\eta$  and  $\eta_0$  denote in the presence and absence of the metal complexes. The value of viscosity was determined from the observed flowing time  $\eta = (t - t_0)/t_0$ . Here  $t$  and  $t_0$  indicate the concentration of DNA with the metal complexes and the metal complexes with respect to time. The relative viscosity of DNA increased during the consecutive addition of complexes to a fixed amount of DNA solution. These data clearly showed that the complexes could bind with DNA through the intercalative binding mode [61].

**DNA damage studies:** DNA cleavage in the presence of only L as well as in the presence of the complexes  $[\text{CuLCl}_2]_2$ ,  $[\text{CoLCl}_2]_2$ ,  $[\text{NiLCl}_2]_2$  and  $[\text{ZnLCl}_2]_2$  was studied using gel electrophoresis and super coiled (SC) plasmid pUC19 DNA in tris-acetate EDTA buffer (pH 7.2). Fig. 12 shows that when circular plasmid DNA was subjected to gel electrophoresis, the intact super coiled form of DNA (Form I) showed the highest mobility. If a nick appeared on one strand, the SC-DNA assumed a relatively slow-moving open circular form (Form II). When both strands of DNA were cleaved, a linear form (Form III)

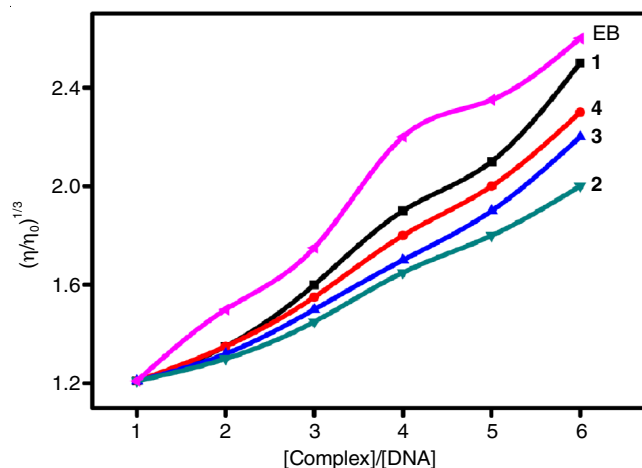


Fig. 11. Effects of increasing amount of classical intercalator [EB] and complexes on the relative viscosity of CT-DNA in 5 mM Tris-HCl/50 mM NaCl buffer at room temperature, where (1) Cu(II), (2) Co(II), (3) Ni(II) and (4) Zn(II) complexes

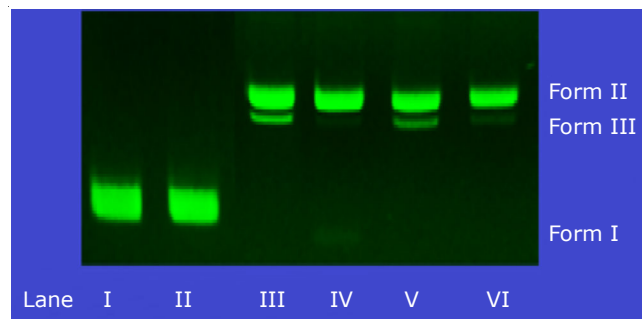


Fig. 12. Gel electrophoresis method of cleavage showing pUC 19 DNA treated with metal complexes: Lane I: DNA control; Lane II: DNA + L +  $\text{H}_2\text{O}_2$ ; Lane III: DNA +  $[\text{CuLCl}_2]_2$  +  $\text{H}_2\text{O}_2$ ; Lane IV: DNA +  $[\text{CoLCl}_2]_2$  +  $\text{H}_2\text{O}_2$ ; Lane V: DNA +  $[\text{NiLCl}_2]_2$  +  $\text{H}_2\text{O}_2$  and Lane VI: DNA +  $[\text{ZnLCl}_2]_2$  +  $\text{H}_2\text{O}_2$

migrated at a speed intermediate to those of Form I and Form II. Unlike the ligand-induced cleavage of plasmid pUC19 DNA, the cleavage of the plasmid induced by synthesized complexes required activators such as hydrogen peroxide [Lanes (III-VI) in Fig. 12]. Under the same conditions, a combination of ligand and  $\text{H}_2\text{O}_2$  did not cleave the pUC19 DNA. These results showed that all the metal complexes efficiently cleaved the DNA from Form I to Form III in the presence of activators such as hydrogen peroxide. The activators generate hydroxyl free radicals that are involved in the oxidation of deoxyribose moiety and hydrolytic cleavage of sugar-phosphate backbone [62]. The copper complex cleaved the pUC19 DNA more easily than the other complexes at the same pH level. The high specificity of copper complex to the pUC19 DNA may be attributable to its high binding efficiency with DNA. This observation implies that DNA alters its conformation due to the binding of dimeric metal(II) complexes. This result indicates that the metal ions play a crucial role in the cleavage of SC-DNA.

**PASS-biological activity assess of ligand:** PASS online software (prediction of activity spectra for biological activity ligand) was used to find out the biological activity of Schiff base ligand. From biological data (Table-7), the synthesized Schiff base ligand shows the biological activity. Ligand acquires most powerful antineoplastic activity for lungs cancer, breast

TABLE-7  
BIOLOGICAL ACTIVITY ASSESSMENT OF SCHIFF BASE LIGAND (L) USING PASS ONLINE SOFTWARE

Pa	Pi	Activity	Pa	Pi	Activity
0.713	0.035	Anti-inflammatory	0.284	0.093	Antituberculosic
0.686	0.017	Analgesic	0.337	0.197	Thromboxane B2 antagonist
0.587	0.032	Antiviral (Picornavirus)	0.279	0.097	Anti-mycobacterial
0.555	0.028	Leucopoiesis inhibitor	0.168	0.036	DNA intercalator
0.516	0.014	Antipyretic	0.320	0.158	Oxygen scavenger
0.511	0.019	Muscular dystrophy treatment	0.223	0.087	Anthelmintic
0.487	0.016	Rheumatoid arthritis treatment	0.232	0.094	Antiparasitic
0.464	0.017	Antineoplastic (colorectal cancer)	0.253	0.136	Antiprotozoal (Coccidial)
0.458	0.018	Antineoplastic (colon cancer)	0.294	0.154	Spermidine dehydrogenase inhibitor
0.417	0.023	Diabetic neuropathy treatment	0.234	0.074	Ferredoxin-nitrite reductase inhibitor
0.463	0.076	Antineoplastic	0.247	0.121	Steroid synthesis inhibitor
0.448	0.078	Thioredoxin inhibitor	0.272	0.144	Anticonvulsant
0.329	0.093	Cytochrome P450 stimulant	0.235	0.095	Cell wall biosynthesis inhibitor
0.336	0.115	Nicotine dehydrogenase inhibitor	0.261	0.172	Cancer associated disorders treatment
0.324	0.073	Lysostaphin inhibitor	0.174	0.092	Antineoplastic (renal cancer)
0.282	0.077	Antineoplastic (breast cancer)	0.187	0.123	Eye irritation, inactive
0.287	0.081	Cytostatic	0.129	0.048	Premenstrual syndrome treatment

Pa = Probability of active; Pi = Probability of inactive.

cancer, renal, colorectal, colon cancer and multiple myeloma. It also possesses potent insulin inhibitor, anti-inflammatory, DNA intercalator, kidney function stimulant, antibacterial, antiviral, antiparasitic, anticonvulsant, antituberculosis, rheumatoid arthritis and diabetic neuropathy treatment.

**in silico ADME-TOX property:** ADME-TOX (absorption, distribution, metabolism, excretion and toxicity) properties of the synthesized Schiff base ligand can be verified by VLS3D (Ligand-based Virtual Screening a Database) software. As per data derived from the online software ligand was easily absorbed in human intestinal cells, where (Pa = 1) and taken into the bloodstream. This implies that it may be useful for the discovery of novel metal-based therapeutic drugs and ligand also carry Pa equal to 0.9857 probabilities, so it moves across the blood-brain barrier (BBB) quickly. This represents it go across the central nervous system readily. It is a non-substrate for CYP450 2C9 and CYP450 2D6 enzymes. It is non-carcinogen and it is having ADME toxic value (Pa) of 0.8765 probabilities.

## Conclusion

A new series of novel Schiff base ligand and its metal complexes of Cu(II), Co(II), Ni(II), and Zn(II) are synthesized and to study their efficacy of DNA binding, DNA cleavage, antimicrobial and cytotoxic activity are also recorded. The synthesized metal complexes are more efficient DNA binders, and the binding properties of the metal complexes were examined by UV absorption spectral studies and viscometric measurements. While all the metal complexes interact with DNA, probably by the intercalation mechanism. The DNA cleavage study was carried out by the gel electrophoresis technique, and the result denotes that copper and cobalt complexes are able to cleave the DNA through double strand helix in the presence of H<sub>2</sub>O<sub>2</sub> activator. The antimicrobial activity of all the metal complexes shows superior antibacterial and antifungal activity related to the free ligand. Thus, this cumulative biological prowess of the metal complexes from present study would be helpful in sensitive of DNA interaction evinced by metal complexes and may lead to establish novel metal-based therapeutic drugs.

## ACKNOWLEDGEMENTS

This work was funded by the Deanship of Scientific Research at Princess Nourah bint Abdulrahman University, through the Research Groups Program Grant number (RGP-1438-00).

## CONFLICT OF INTEREST

The authors declare that there is no conflict of interests regarding the publication of this article.

## REFERENCES

- M. Nath and P.K. Saini, *Dalton Trans.*, **40**, 7077 (2011); <https://doi.org/10.1039/c0dt01426e>.
- P.G. Cozzi, *Chem. Soc. Rev.*, **33**, 410 (2004); <https://doi.org/10.1039/B307853C>.
- N. Ananthi, U. Balakrishnan, S. Velmathi, K.B. Manjunath and G. Umesh, *Opt. Photonics J.*, **2**, 40 (2012); <https://doi.org/10.4236/opj.2012.21006>.
- R. Antony, S.T. David Manickam, P.V. Chandrasekar, K. Karuppasamy, P. Kollu and S. Balakumar, *RSC Adv.*, **4**, 24820 (2014); <https://doi.org/10.1039/C4RA01960A>.
- M. Abu-Dief and I.M.A. Mohamed, *Beni-Suef Univ. J. Basic Appl. Sci.*, **4**, 119 (2015); <https://doi.org/10.1016/j.bjbas.2015.05.004>.
- A. Kundu, P.S. Hariharan, K. Prabakaran and S.P. Anthony, *Sens. Actuators B Chem.*, **206**, 524 (2015); <https://doi.org/10.1016/j.snb.2014.09.099>.
- H.K. Liu and P.J. Sadler, *Acc. Chem. Res.*, **44**, 349 (2011); <https://doi.org/10.1021/ar100140e>.
- U. Jungwirth, C.R. Kowol, B.K. Keppler, C.G. Hartinger, W. Berger and P. Hellfetter, *Antioxid. Redox Signal.*, **15**, 1085 (2011); <https://doi.org/10.1089/ars.2010.3663>.
- S.L.H. Higgins, T.A. White, B.S.J. Winkel and K.J. Brewer, *Inorg. Chem.*, **50**, 463 (2011); <https://doi.org/10.1021/ic100958r>.
- S. Kathiresan, S. Mugesh, J. Annaraj and M. Murugan, *New J. Chem.*, **41**, 1267 (2017); <https://doi.org/10.1039/C6NJ03501A>.
- N. Raman, M. Selvaganapathy and S. Radhakrishnan, *Spectrochim. Acta A Mol. Biomol. Spectrosc.*, **127**, 185 (2014); <https://doi.org/10.1016/j.saa.2014.02.018>.
- M. Shamsi, S. Yadav and F. Arjmand, *J. Photochem. Photobiol. B*, **136**, 1 (2014); <https://doi.org/10.1016/j.jphotobiol.2014.04.009>.

13. P. Gurumoorthy, D. Mahendiran, D. Prabhu, C. Arulvasu and A.K. Rahiman, *RSC Adv.*, **4**, 42855 (2014); <https://doi.org/10.1039/C4RA06941B>.
14. G. Dehghan, J.E.N. Dolatabadi, A. Jouyban, K.A. Zeinali, S.M. Ahmadi and S. Kashaman, *DNA Cell Biol.*, **30**, 95 (2011); <https://doi.org/10.1089/dna.2010.1063>.
15. G. Zuber, J.C. Quada and S.M. Hecht, *J. Am. Chem. Soc.*, **120**, 9368 (1998); <https://doi.org/10.1021/ja981937r>.
16. T. Punniyamurthy, S.J.S. Kalra and J. Iqbal, *Tetrahedron Lett.*, **36**, 8497 (1995); [https://doi.org/10.1016/0040-4039\(95\)01780-L](https://doi.org/10.1016/0040-4039(95)01780-L).
17. R.K. Agarwal, L. Singh and D.K. Sharma, *Bioinorg. Chem. Appl.*, **Article ID 59509** (2006); <https://doi.org/10.1155/BCA/2006/59509>.
18. S. Gopalakrishnan and J. Joseph, *Mycobiology*, **37**, 141 (2009); <https://doi.org/10.4489/MYCO.2009.37.2.141>.
19. C.A. Contreras-Celedón, J.A. Rincón-Medina, D. Mendoza-Rayó and L. Chacón-García, *Appl. Organomet. Chem.*, **29**, 439 (2015); <https://doi.org/10.1002/aoc.3312>.
20. V. Arun, N. Sridevi, P.P. Robinson, S. Manju and K.K.M. Yusuff, *J. Mol. Catal. A*, **304**, 191 (2009); <https://doi.org/10.1016/j.molcata.2009.02.011>.
21. C.A. Contreras-Celedón, D. Mendoza-Rayó, J.A. Rincón-Medina and L. Chacón-García, *Beilstein J. Org. Chem.*, **10**, 2821 (2014); <https://doi.org/10.3762/bjoc.10.299>.
22. K. Satyanarayana and M.N.A. Rao, *Eur. J. Med. Chem.*, **30**, 641 (1995); [https://doi.org/10.1016/0223-5234\(96\)88280-8](https://doi.org/10.1016/0223-5234(96)88280-8).
23. I.V. Shemarova, E.B. Maizel, I.V. Voznyi, N.P. Stepanova and A.E. Khovanskikh, *Pharm. Chem. J.*, **34**, 530 (2000); <https://doi.org/10.1023/A:1010355129735>.
24. N. Raman, S.J. Raja and A. Sakthivel, *J. Coord. Chem.*, **62**, 691 (2009); <https://doi.org/10.1080/00958970802326179>.
25. R. Antony, S.T.D. Manickam, K. Karuppasamy, P.V. Chandrasekar, P. Kollu and S. Balakumar, *RSC Adv.*, **4**, 42816 (2014); <https://doi.org/10.1039/C4RA08303B>.
26. D. Kivelson and R. Neiman, *J. Chem. Phys.*, **35**, 149 (1961); <https://doi.org/10.1063/1.1731880>.
27. B.J. Hathaway and D.E. Billing, *Coord. Chem. Rev.*, **5**, 143 (1970); [https://doi.org/10.1016/S0010-8545\(00\)80135-6](https://doi.org/10.1016/S0010-8545(00)80135-6).
28. Y. Zhou, H. Zhou, J. Zhang, L. Zhang and J. Niu, *Mol. Biomol. Spect.*, **98**, 14 (2012); <https://doi.org/10.1016/j.saa.2012.08.025>.
29. J.B. Chaires, N. Dattagupta and D.M. Crothers, *Biochemistry*, **21**, 3933 (1982); <https://doi.org/10.1021/bi00260a005>.
30. Y. Li, G. Zhang and M. Tao, *J. Photochem. Photobiol. B*, **138**, 109 (2014); <https://doi.org/10.1016/j.jphotobiol.2014.05.011>.
31. A.K. Sadana, Y. Mirza, K.R. Aneja and O. Prakash, *Eur. J. Med. Chem.*, **38**, 533 (2003); [https://doi.org/10.1016/S0223-5234\(03\)00061-8](https://doi.org/10.1016/S0223-5234(03)00061-8).
32. A. van Tonder, A.M. Joubert and A.D. Cromarty, *BMC Res. Notes*, **8**, 47 (2015); <https://doi.org/10.1186/s13104-015-1000-8>.
33. E.E. Oruç, S. Rollas, F. Kandemirli, N. Shvets and A.S. Dimoglo, *J. Med. Chem.*, **47**, 6760 (2004); <https://doi.org/10.1021/jm0495632>.
34. T. Sander, J. Freyss, M. von Korff, J.R. Reich and C. Rufener, *J. Chem. Inf. Model.*, **49**, 232 (2009); <https://doi.org/10.1021/ci800305f>.
35. M.D. Segall, A.P. Beresford, J.M.R. Gola, D. Hawksley and M.H. Tarbit, *Expert Opin. Drug Metab. Toxicol.*, **2**, 325 (2006); <https://doi.org/10.1517/17425255.2.2.325>.
36. B. Mathew, J. Suresh and S. Anbazhagan, *Biomed. Aging Pathol.*, **4**, 327 (2014); <https://doi.org/10.1016/j.biomag.2014.08.002>.
37. F. Liu and B. Fang, *Chin. J. Biotechnol.*, **23**, 133 (2007); [https://doi.org/10.1016/S1872-2075\(07\)60012-0](https://doi.org/10.1016/S1872-2075(07)60012-0).
38. J.R. Durig, J.J. Klaassen, B.S. Deodhar, T.K. Gounev, A.R. Conrad and M.J. Tubergen, *Spectrochim. Acta A*, **87**, 214 (2012); <https://doi.org/10.1016/j.saa.2011.11.041>.
39. A.A. Abou-Hussein and W. Linert, *Spectrochim. Acta A Mol. Biomol. Spectrosc.*, **117**, 763 (2014); <https://doi.org/10.1016/j.saa.2013.06.078>.
40. E.M. Zayed, A.M.M. Hindy and G.G. Mohamed, *Appl. Organomet. Chem.*, **32**, e3952 (2018); <https://doi.org/10.1002/aoc.3952>.
41. M.M. Omar, G.G. Mohamed and A.A. Ibrahim, *Spectrochim. Acta A Mol. Biomol. Spectrosc.*, **73**, 358 (2009); <https://doi.org/10.1016/j.saa.2009.02.043>.
42. G.G. Mohamed, M.M. Omar and A.A. Ibrahim, *Eur. J. Med. Chem.*, **44**, 4801 (2009); <https://doi.org/10.1016/j.ejmech.2009.07.028>.
43. N. Raman, K. Pothiraj and T. Baskaran, *J. Coord. Chem.*, **64**, 3900 (2011); <https://doi.org/10.1080/00958972.2011.634005>.
44. S. Srinivasan, P. Athappan and G. Rajagopal, *Transition Met. Chem.*, **26**, 588 (2001); <https://doi.org/10.1023/A:1011007429295>.
45. C.X. Zhang and S.J. Lippard, *Curr. Opin. Chem. Biol.*, **7**, 481 (2003); [https://doi.org/10.1016/S1367-5931\(03\)00081-4](https://doi.org/10.1016/S1367-5931(03)00081-4).
46. R.F. Brissos, E. Torrents, F.M. dos Santos Mello, W. Carvalho-Pires, E. de Paula Silveira-Lacerda, A.B. Caballero, A. Caubet, C. Massera, O. Rubeau, S.J. Teat and P. Gamez, *Metallomics*, **6**, 1853 (2014); <https://doi.org/10.1039/C4MT00152D>.
47. D. Kivelson and R. Neiman, *J. Chem. Phys.*, **35**, 149 (1961); <https://doi.org/10.1063/1.1731880>.
48. P. Priya, S.V. Arunachalam, N. Sathya, C. Jayabalakrishnan and V. Chinnusamy, *Transition Met. Chem.*, **34**, 437 (2009); <https://doi.org/10.1007/s11243-009-9214-z>.
49. S. Sarkar, A. Mondal, M.S. El Fallah, J. Ribas, D. Chopra, H. Stoeckli-Evans and K.K. Rajak, *Polyhedron*, **25**, 25 (2006); <https://doi.org/10.1016/j.poly.2005.06.059>.
50. M.S. El-Shahawi and A.F. Shoir, *Spectrochim. Acta A Mol. Biomol. Spectrosc.*, **60**, 121 (2004); [https://doi.org/10.1016/S1386-1425\(03\)00191-4](https://doi.org/10.1016/S1386-1425(03)00191-4).
51. A.W. Coats and J.P. Redfern, *Nature*, **201**, 68 (1964); <https://doi.org/10.1038/201068a0>.
52. H.H. Horowitz and G. Metzger, *Anal. Chem.*, **35**, 1464 (1963); <https://doi.org/10.1021/ac60203a013>.
53. G.O. Piloyan, I.D. Ryabchikov and O.S. Novikova, *Nature*, **212**, 1229 (1966); <https://doi.org/10.1038/2121229a0>.
54. H. Chen, J.A. Parkinson, R.E. Morris and P.J. Sadler, *J. Am. Chem. Soc.*, **125**, 173 (2003); <https://doi.org/10.1021/ja027719m>.
55. V.G. Vaidyanathan and B.U. Nair, *Eur. J. Inorg. Chem.*, **9**, 1840 (2004); <https://doi.org/10.1002/ejic.200300718>.
56. F.A. Beckford, M. Shalowski Jr., G. Leblanc, J. Thessing, L.C. Lewis-Alleyne, A.A. Holder, L. Li and N.P. Seeram, *Dalton Trans.*, 10757 (2009); <https://doi.org/10.1039/b915081a>.
57. V.L. Kinnula and J.D. Crapo, *Free Radic. Biol. Med.*, **36**, 718 (2004); <https://doi.org/10.1016/j.freeradbiomed.2003.12.010>.
58. H.F. Abd El Halim and G.G. Mohamed, *Appl. Organomet. Chem.*, **32**, e4176 (2017); <https://doi.org/10.1002/aoc.4176>.
59. S.K. Mal, M. Mitra, G. Kaur, V.M. Manikandamathavan, M.S. Kiran, A.R. Choudhury, B.U. Nair and R. Ghosh, *RSC Adv.*, **4**, 61337 (2014); <https://doi.org/10.1039/C4RA09448D>.
60. W.D. Wilson, L. Ratmeyer, M. Zhao, L. Strekowski and D. Boykin, *Biochemistry*, **32**, 4098 (1993); <https://doi.org/10.1021/bi00066a035>.
61. V.A. Kawade, A.A. Kumbhar, A.S. Kumbhar, C. Näther, A. Erxleben, U.B. Sonawane and R.R. Joshi, *Dalton Trans.*, **40**, 639 (2011); <https://doi.org/10.1039/C0DT01078B>.
62. J. Liu, W. Zheng, S. Shi, C. Tan, J. Chen, K. Zheng and L. Ji, *J. Inorg. Biochem.*, **102**, 193 (2008); <https://doi.org/10.1016/j.jinorgbio.2007.07.035>.